Convergent immunological solutions to Argentine hemorrhagic fever virus neutralization

Antra Zeltina[a], Stefanie A. Krumm[b], Mehmet Sahin[c], Weston B. Struwe[d], Karl Harlos[a], Jack H. Nunberg[e], Max Crispin[d,f], Daniel D. Pinschewer[c], Katie J. Doores[b,1], and Thomas A. Bowden[a,1]

[a]Division of Structural Biology, Wellcome Trust Centre for Human Genetics, University of Oxford, Oxford OX3 7BN, United Kingdom; [b]Department of Infectious Diseases, Guy's Hospital, King's College London, London SE1 9RT, United Kingdom; [c]Division of Experimental Virology, Department of Biomedicine, University of Basel, Basel CH-4051, Switzerland; [d]Oxford Glycobiology Institute, Department of Biochemistry, University of Oxford, Oxford OX1 3QU, United Kingdom; [e]Montana Biotechnology Center, University of Montana, Missoula, MT 59812; and [f]Department of Immunology and Microbial Science, The Scripps Research Institute, La Jolla, CA 92037

Edited by Pamela J. Bjorkman, California Institute of Technology, Pasadena, CA, and approved May 23, 2017 (received for review February 10, 2017)

Transmission of hemorrhagic fever New World arenaviruses from their rodent reservoirs to human populations poses substantial public health and economic dangers. These zoonotic events are enabled by the specific interaction between the New World arenaviral attachment glycoprotein, GP1, and cell surface human transferrin receptor (hTfR1). Here, we present the structural basis for how a mouse-derived neutralizing antibody (nAb), OD01, disrupts this interaction by targeting the receptor-binding surface of the GP1 glycoprotein from Junín virus (JUNV), a hemorrhagic fever arenavirus endemic in central Argentina. Comparison of our structure with that of a previously reported nAb complex (JUNV GP1–GD01) reveals largely overlapping epitopes but highly distinct antibody-binding modes. Despite differences in GP1 recognition, we find that both antibodies present a key tyrosine residue, albeit on different chains, that inserts into a central pocket on JUNV GP1 and effectively mimics the contacts made by the host TfR1. These data provide a molecular-level description of how antibodies derived from different germline origins arrive at equivalent immunological solutions to virus neutralization.

arenavirus | glycoprotein | structure | antibody response | hemorrhagic fever

New World (NW) clade B arenaviruses (genus *Mammarenavirus*) comprise a number of human pathogens, including Junín virus (JUNV), Machupo virus (MACV), and Guanarito virus (1, 2). These viruses are endemic to rodent populations in rural areas of Argentina, Bolivia, and Venezuela, respectively, and viral spillover into human populations can result in severe hemorrhagic fever (HF) (3). Novel pathogenic NW arenaviruses continue to be identified (4–6), underscoring a wide-scale need for effective vaccines and therapeutics.

JUNV, the etiological agent of Argentine hemorrhagic fever (AHF), constitutes one of the most dangerous NW arenaviruses, putting an estimated 5 million people at risk (7, 8). JUNV infection typically exhibits a rapid onset of disease (7–14 d) and high mortality rates (15–30%) (7, 9, 10). There are no internationally approved drugs for preventing or treating NW arenavirus HF. However, the successful development of a live, attenuated JUNV vaccine, Candid#1, has proven that AHF can be controlled (11). Similarly, virus-neutralizing immune plasma from convalescent individuals has been successfully used for the treatment of AHF (10, 12).

The JUNV envelope surface is decorated by trimeric multifunctional glycoprotein complex (GPC) spikes. Each protomer in the trimer consists of: a myristoylated (13) stable signal peptide, an attachment subunit (GP1), and a transmembrane fusion subunit (GP2) (14–19). Host-cell entry of JUNV and other clade B arenaviruses is initiated by the interaction between the arenaviral GP1 and the host transferrin receptor (TfR1) (20). The GP1 subunit interacts with the apical domain of TfR1, distal from natural transferrin and hereditary hemochromatosis protein recognition sites (21, 22). A primary determinant of zoonotic spread of clade B arenaviruses is the ability of the GP1 to recognize the human TfR1 ortholog (20, 23).

The JUNV GPC spike comprises the primary target for neutralizing immune responses (24) and three GPC-specific mouse-derived nAbs—GD01, OD01, and GB03—have shown promise in animal models of infection (25), raising hopes for the development of mAb-based therapeutics. The structural basis for virus neutralization by one such mAb, GD01, has been elucidated, revealing an epitope on the GP1 glycoprotein that overlaps with the hTfR1 binding site (26). Here, we sought to determine the molecular basis for JUNV neutralization by the similarly derived mAb OD01. Our X-ray crystallographic investigation reveals that although OD01 bears highly contrasting paratopes and exhibits a smaller binding surface on JUNV GP1 than GD01, both antibodies effectively mimic the contacts made by the host TfR1 during viral attachment. This analysis demonstrates that antibodies derived from different germlines can achieve this highly effective immunological solution.

Results

Structure Determination of JUNV GP1–OD01 Fab Complex. The mouse-derived neutralizing antibody, OD01 (clone OD01-AA09), has been shown to target the glycoprotein spike of JUNV (24). To refine the specificity of the nAb OD01, we performed an ELISA using our recombinantly derived JUNV GP1 (residues D87–V231) as an antigen (Fig. 1*A*). Although nAb OD01 bound

Significance

An estimated 5 million people are at risk of infection by Junín virus (JUNV), the causative agent of Argentine hemorrhagic fever. JUNV displays a glycoprotein spike complex on the surface of the viral envelope that is responsible for negotiating host-cell recognition and entry. Herein, we show that monoclonal antibodies that have gone through different germline selection pathways have converged to target the host-cell receptor-binding site on the JUNV glycoprotein spike. Immunofocusing of the antibody response to mimic natural host–receptor interactions reveals a key point of vulnerability on the JUNV surface.

Author contributions: A.Z., S.A.K., J.H.N., K.J.D., and T.A.B. designed research; A.Z., S.A.K., K.H., K.J.D., and T.A.B. performed research; A.Z., S.A.K., M.S., W.B.S., J.H.N., M.C., D.D.P., K.J.D., and T.A.B. analyzed data; and A.Z., S.A.K., M.S., W.B.S., K.H., J.H.N., M.C., D.D.P., K.J.D., and T.A.B. wrote the paper.

The authors declare no conflict of interest.

This article is a PNAS Direct Submission.

Data deposition: The atomic coordinates and structure factors have been deposited in the Protein Data Bank, www.pdb.org (PDB ID code 5NUZ).

[1]To whom correspondence may be addressed. Email: katie.doores@kcl.ac.uk or thomas.bowden@strubi.ox.ac.uk.

This article contains supporting information online at www.pnas.org/lookup/suppl/doi:10.1073/pnas.1702127114/-/DCSupplemental.

to JUNV GP1 at concentrations as low as 0.01 μg·mL^{-1}, no cross-reactivity was observed with MACV GP1 or the lymphocytic choriomeningitis virus (LCMV) GP1-negative control. To facilitate structure determination, recombinant JUNV GP1 (Fig. 1*B*) was deglycosylated with endoglycosidase F_1 (endoF_1) (*SI Appendix*, Fig. S1*A*) and crystallized in complex with the antigen-binding fragment (Fab) of OD01. The structure of the complex was solved to 1.95-Å resolution (*SI Appendix*, Table S1). The amino acid sequence of OD01 was predicted crystallographically and used to create an engineered Fab fragment (herein referred to as eOD01) capable of stably and specifically binding JUNV GP1 (*SI Appendix*, Figs. S1 *B* and *C* and S2). Recombinant expression, crystallization, and structural determination of eOD01 with JUNV GP1 to 1.85-Å resolution (Fig. 1*C* and *SI Appendix*, Table S1) revealed identical binding modes for the JUNV GP1–OD01 and JUNV GP1–eOD01 complexes (0.2 Å rmsd over 569 Cα residues) (*SI Appendix*, Fig. S3). We note that it is possible for subtle amino acid sequence differences that could not be distinguished by crystallographic analysis at this resolution (e.g., Asn vs. Asp) to exist between OD01 and our engineered version. However, the near identical mode of JUNV GP1 recognition provides a realistic model for JUNV neutralization by the native antibody.

Structural Characterization of JUNV GP1–eOD01. Two JUNV GP1–eOD01 Fab complexes were present in the asymmetric unit, with minimal structural differences observed between crystallographically related JUNV GP1 and eOD01 Fab pairs (*SI Appendix*, Fig. S4 *A* and *B*). As previously observed (26), JUNV GP1 forms a compact α/β-fold (Fig. 1*B*). The two eOD01 Fabs in the asymmetric unit recognize JUNV GP1 nearly identically, with both binding to the convex face of their cognate GP1 molecules at a site overlapping that used for TfR1 attachment (Fig. 1 *C* and *D*) (0.6 Å rmsd over 575 equivalent JUNV GP1–eOD01 complex Cα atoms) (*SI Appendix*, Fig. S4*C*). The JUNV GP1–eOD01 interaction interface occludes ~1,200 Å^2 of solvent-accessible surface area. Complementarity-determining regions (CDRs) from both the heavy and light chains of eOD01 form contacts with JUNV GP1, indicating that the chains are likely to be mutually required for antigen recognition (Figs. 1*C* and 2*A* and Table 1).

Although the heavy-chain CDR loops H2 and, especially, H3 make a sizeable contribution to the eOD01–GP1 interface, the interaction is dominated by the CDR1 from the light chain (CDR L1), which extends a 15-amino acid loop deep into a central pocket on the β-sheet of JUNV GP1 (Figs. 1*C* and 2*A*). Tyr30B from eOD01 CDR L1 [Chothia numbering scheme (27)] appears to be of chief importance to this interface, where the side-chain hydroxyl group hydrogen bonds with JUNV GP1 side-chains Ser111 and Asp113 at the tip of the third strand of JUNV GP1 (Fig. 2*A*). From the opposite side of the central pocket, the Tyr30B^{eOD01} main chain is stabilized by an additional hydrogen-bonding interaction with the guanidinium group of Arg165$^{JUNV\ GP1}$ (Fig. 2*A*). Additionally, the aromatic ring of Tyr30B^{eOD01} is surrounded by the side chains of Ile115$^{JUNV\ GP1}$, Val117$^{JUNV\ GP1}$, Ile174$^{JUNV\ GP1}$, and Lys216$^{JUNV\ GP1}$, which contribute to the hydrophobicity of the pocket (*SI Appendix*, Fig. S5).

Although *N*-linked glycans decorate the periphery of the JUNV GP1 β-sheet (Fig. 1*B*), the crystallographically observed antibody–antigen interaction is predominantly carbohydrate

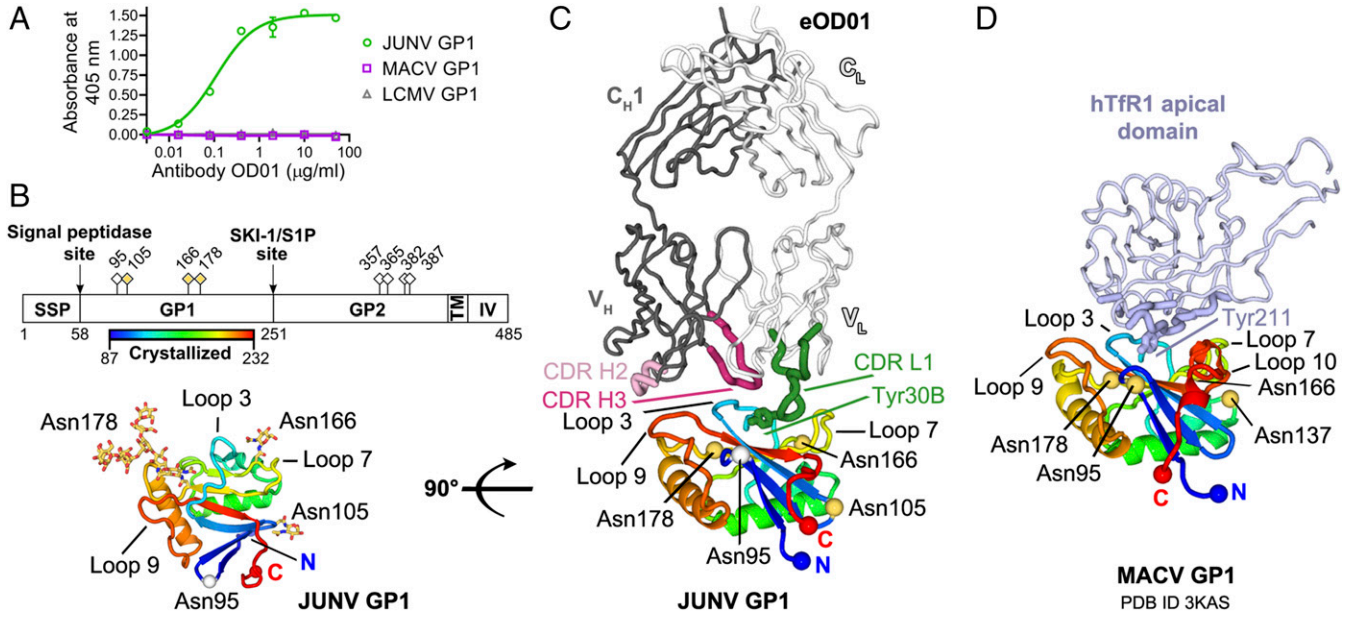

Fig. 1. Reactivity and binding mode of the JUNV-specific neutralizing antibody, OD01. (*A*) ELISA analysis of nAb OD01 titrated against immobilized arenavirus GP1 glycoproteins. Wells were coated with JUNV GP1, MACV GP1, or LCMV GP1 (negative control). Error bars, SD ($n = 3$), not shown when smaller than symbol size. (*B*, *Upper*) Domain organization of the JUNV glycoprotein precursor [produced using the DOG software (53)]. The JUNV GP1 construct used for crystallization is highlighted as a rainbow. Diamond-shaped symbols designate *N*-linked glycosylation sequons (NXT/S, where X ≠ P) with sites observed to be occupied in the crystal structure colored yellow. GP1, attachment glycoprotein; GP2, fusion glycoprotein; IV, intravirion domain; SKI-1/S1P, subtilisin-like kexin protease-1/site-1-protease; SSP, stable signal peptide; TM, transmembrane domain. (*Lower*) JUNV GP1 from the JUNV GP1–Fab eOD01 cocrystal structure. JUNV GP1 is shown as a cartoon and colored as a rainbow ramped from blue (N terminus) to red (C terminus). Primary interaction loops involved in eOD01 binding are labeled and *N*-linked glycans are shown as sticks. Glycosylation was not detected at Asn95, which is indicated as a white sphere. (*C*) Structure of JUNV GP1 in complex with eOD01. CDRs contributing to JUNV recognition are colored pink (heavy chain) and green (light chain). The side chain from residue Tyr30B of the eOD01 light chain is shown in stick representation. V_H, V_L, C_H1, and C_L denote the antibody variable heavy, variable light, constant heavy 1, and constant light-chain domains, respectively. The positions of crystallographically observed *N*-linked glycosylation on JUNV GP1 are indicated as yellow spheres. (*D*) Structure of MACV GP1 in complex with hTfR1 (22). Only the apical domain of hTfR1 (blue) is shown for clarity. Regions of hTfR1 that interact with MACV are marked as thick tubes and the side chain from the conserved tyrosine residue, Tyr211, is shown in stick representation.

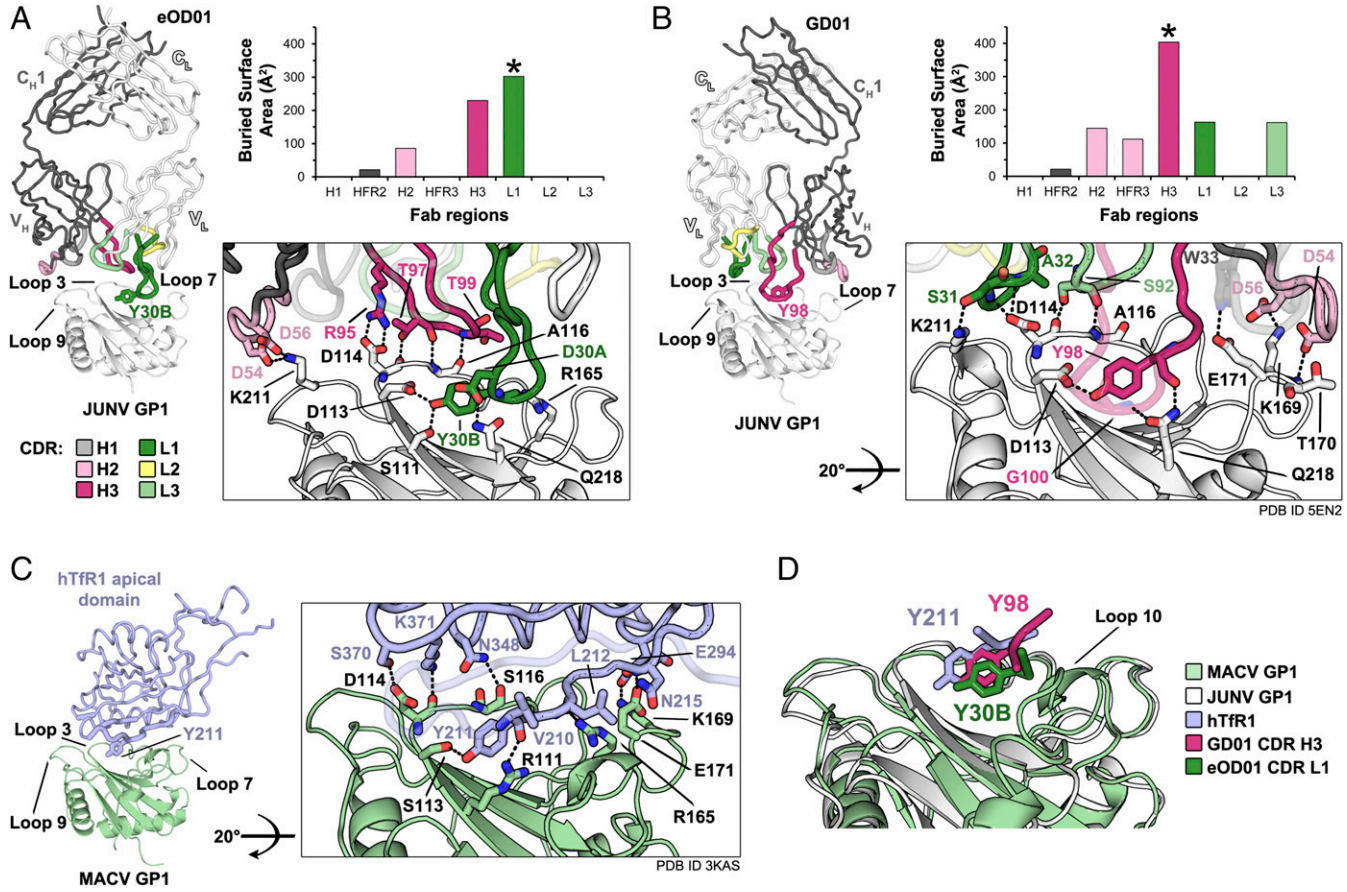

Fig. 2. Comparison of the JUNV GP1–eOD01, JUNV GP1–GD01, and MACV GP1–hTfR1 complex interfaces. (*A*, *Left*) Interaction between JUNV GP1 and eOD01. JUNV GP1 is shown as a gray cartoon, CDR loops of eOD01 are colored as indicated [Chothia numbering scheme (27)]. V_H, V_L, C_H1, and C_L denote the antibody variable heavy, variable light, constant heavy 1, and constant light-chain domains, respectively. (*Upper Right*) CDR loop use by eOD01 in the JUNV GP1 complex with the CDR loop carrying Y30B denoted with an asterisk; calculated using the PDBePISA server (54) and measured in buried surface area (Å^2). (*Lower Right*) Close-up view of the JUNV GP1–eOD01 interface with intermolecular hydrogen bonds (distance ≤ 3.5 Å) highlighted with dashes and the participating residues shown as sticks. (*B*, *Left*) Structure of JUNV GP1 in complex with GD01 (26), as presented in *A*. (*Upper Right*) CDR loop use by GD01 in the JUNV GP1 complex with the CDR loop carrying Y98 denoted with an asterisk, calculated as in *A* (54). (*Lower Right*) Close-up view of the JUNV GP1–GD01 interface. Hydrogen bonds formed by the same JUNV GP1 residues as in *A* are shown, as well as bonds involving the JUNV GP1 loop 7. (*C*) Interaction between the apical domain of hTfR1 (blue) in complex with MACV GP1 (22) (pale green), with zoom-in panel as presented in *B*. (*D*) Relative orientation of the $Y211^{hTfR1}$ (blue), $Y98^{GD01\ CDRH3}$ (pink), and $Y30B^{eOD01\ CDRL1}$ (dark green) residues with respect to JUNV GP1 (white cartoon) and MACV GP1 (pale green cartoon).

independent (*SI Appendix*, Fig. S4*C*). Electron density corresponding to at least one GlcNAc moiety was observed at three of the four *N*-linked glycosylation sequons: Asn105, Asn166, Asn178, but not Asn95. A chain of at least six *N*-linked glycan moieties ($Man_4GlcNAc_2$) was ordered at Asn178 in both molecules of the asymmetric unit, suggestive that the di-*N*-acetylchitobiose core of this glycan is protected by the surrounding proteinous environment from endoF_1 digestion (Fig. 1*B* and *SI Appendix*, Fig. S6*A*). Upon overlay, we note that the extensions of the Asn178 glycans form subtly different conformations in the two molecules of the asymmetric unit (*SI Appendix*, Fig. S6*B*), indicating that differential packing environments may play a role in stabilizing the termini of these otherwise flexible glycans.

Table 1. Comparison of JUNV GP1–eOD01 and JUNV GP1–GD01 interfaces

Antibody properties	eOD01 heavy chain	eOD01 light chain	GD01 heavy chain	GD01 light chain
Amino acid length of CDR loops	H1: 7 (94%)*	L1: 15 (9%)*,†	H1: 7 (94%)*	L1: 11 (31%)*
	H2: 6 (81%)*	L2: 7 (99%)*	H2: 6 (81%)*	L2: 7 (99%)*
	H3: 11 (13%)*	L3: 9 (77%)*	H3: 15 (1%)*,†	L3: 9 (77%)*
Footprint on JUNV GP1, Å^2‡	~400	~200	~600	~300
JUNV GP1 residues contacted‡,§	11	10	21	11
Hydrogen bonds‡,§	7	4	13	7

*Values in parenthesis indicate the frequency of the particular CDR loop length in *Mus musculus*, calculated using the abYsis system (29).
†Dominant paratopes in each respective Fab.
‡Calculated using the PDBePISA server (54).
§Calculations done for the JUNV GP1-eOD01 complex 1, as defined in the legend to *SI Appendix*, Fig. S4.

Although glycans do not appear to play a role in eOD01–JUNV GP1 complex formation, the presence of glycosylation on the GP1 does affect the potency of antibody-mediated neutralization. For example, OD01 and GD01 neutralize rLCMV displaying an XJ Clone 3 JUNV vaccine strain glycoprotein, which lacks the Asn166 glycosylation motif, more potently than the autologous virus, in which this glycosylation motif has been restored (28). Considering the proximity of Asn166 to the JUNV GP1–antibody interface (Fig. 1*C*), it seems possible that the presence of native *N*-linked glycosylation at this site may interfere with the antibody–glycoprotein interaction.

eOD01 and GD01 Are Distinct yet Target Overlapping Epitopes. The structure of GD01 in complex with JUNV GP1 has been previously reported (26) and provides an opportunity to compare how JUNV is neutralized by two unique mouse-derived anti-JUNV nAbs (Figs. 2 *A* and *B* and 3 and Table 1). Structural comparison of these two complexes reveals that the antibodies exhibit differing footprint sizes on the GP1 surface (~600 and ~900 Å^2 for eOD01 and GD01, respectively), with both epitopes overlapping the predicted receptor binding site (RBS). Despite contacting the same region of the JUNV GP1 surface, the two nAbs exhibit highly contrasting modes of antigen recognition, where the light- and heavy-chain epitopes on JUNV GP1 are largely swapped (Figs. 2 *A* and *B* and 3). For example, GP1 loop 3 residues Asp114 and Ala116 are stabilized by intermolecular hydrogen bonds in both GP1–nAb complexes. However, although these interactions are mediated by nAb heavy-chain residues Arg95, Thr97, and Thr99 in the GP1–eOD01 complex, light-chain residues Ser31, Ala32, and Ser92 provide these contacts in the GP1–GD01 interface (Fig. 2 *A* and *B*).

These contrasting modes of antigen recognition are reflected in the amino acid length and sequence of the dominant CDR regions (Table 1 and *SI Appendix*, Figs. S7 and S8). For example, whereas the CDR L1 loop of eOD01 is 15 amino acids in length, characteristic of the mouse *IGKV3* germline family, the corresponding CDR L1 region of GD01 is derived from a different mouse germline group *IGKV6* and is 11 amino acids (*SI Appendix*, Fig. S7), a length more commonly observed both in mouse and human antibodies (29) (Table 1). Interestingly, the eOD01 light-chain protein sequence shows little deviation from the germline *IGKV3-2*01* V-gene (*SI Appendix*, Fig. S7), with only one mutation in the CDR L1 region. Instead of CDR L1, the GD01–GP1 interaction is dominated by the 15-amino acid CDR H3, which is uncommonly long for the species, with only ~3% of the sequenced mouse CDR H3s displaying a length equal to or greater than 15 amino acids (29) (Table 1).

A Shared Feature of Receptor Mimicry. We note a striking commonality between eOD01 and GD01: Tyr30B from the L1 loop of eOD01 occupies a position in the central pocket of JUNV GP1 that largely overlaps with that of Tyr98 from the CDR H3 loop of GD01 (Fig. 2 *A* and *B*). This position is also highly similar to the location of Tyr211^{hTfR1} in the MACV GP1–hTfR1 complex (22) (Fig. 2 *C* and *D*), the only clade B arenavirus glycoprotein–receptor structure reported to date. Tyr211 is a key residue in the GP1–hTfR1 interface (22) and conserved across all TfR1 orthologs that support NW arenavirus entry (23, 30, 31). Although we note that sequence and structural variation between the MACV GP1 and JUNV GP1 RBS exist, the colocalization of Tyr30B^{eOD01} and Tyr98^{GD01} at the Tyr211^{hTfR1} recognition site indicates that both nAbs effectively mimic TfR1-mediated arenaviral attachment.

Discussion

NW hemorrhagic fever arenaviruses pose a significant threat to human health, underscoring the need for effective vaccines and antiviral therapies. Although practical limitations of convalescent serum therapy exist, passive transfer of immunoglobulins remains an effective AHF treatment in a postexposure context (10, 12), confirming that the neutralizing antibody response is crucial for controlling JUNV infection.

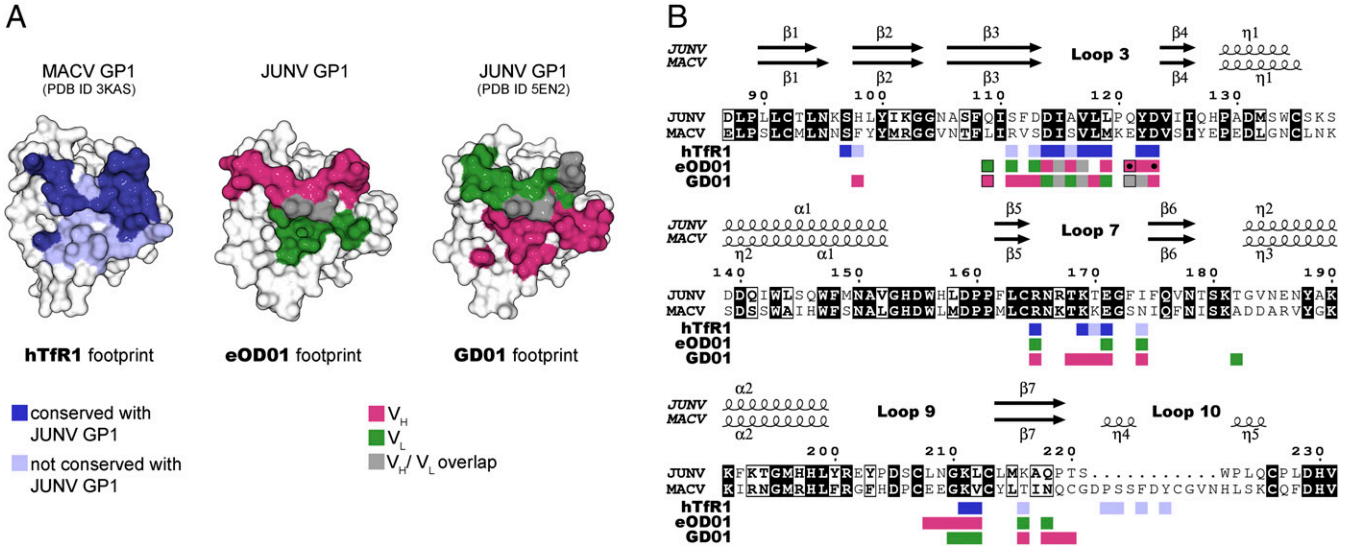

Fig. 3. Footprints of hTfR1, eOD01, and GD01 plotted onto MACV and JUNV GP1. (*A*) Surface representations of MACV GP1 (*Left*) and JUNV GP1 (*Center* and *Right*). The footprint of hTfR1 on MACV GP1 is shown in blue. Dark blue represents amino acid residues conserved between MACV GP1 and JUNV GP1 (both identical and similar residues); not conserved residues are in light blue (including deletions and insertions). The antibody heavy (V_H) and light (V_L) chain footprints on JUNV GP1 are colored pink and green, respectively. Residues contacted by both chains are shown in gray. (*B*) Sequence alignment of JUNV GP1 residues 87–231 with the corresponding residues of the MACV GP1 [determined by Clustal Omega (55), plotted by ESPript (56), and adjusted by hand]. Secondary structure elements are shown with arrows representing β-strands (β1–β7) and spirals representing α (α1–2) and 3_{10}-helices (η1–5). Colored squares under the sequence alignment mark GP1 residues contacted by hTfR1, eOD01, and GD01; colored as in *A*. Black-bordered squares indicate residues not conserved between the JUNV GP1 sequences used for cocrystallization with OD01 (shown) and GD01 (i.e., Q109K and Q121E). Black dots denote JUNV GP1 residues forming minor contacts with eOD01, which were only observed in one of the two complexes in the asymmetric unit.

Our structural analysis reveals that antibodies derived from different germlines can be directed to mimic host–receptor interactions on JUNV GP1. Similarly, neutralizing RBS-targeting antibodies of differing germline origins have been observed in other viruses, including influenza virus, HIV, and poliovirus (32–34). In the case of influenza virus, it has been possible to recognize a signature binding motif on the CDR H3 loop (33). Here, we demonstrate that a key immunoglobulin tyrosine residue, which mimics the critical $Tyr211^{hTfR1}$, can be located on the CDR loops of either heavy or light chains of anti-JUNV nAbs.

Although our structural analysis suggests that nAbs use the functionally conserved TfR1 binding site on the NW arenaviral GP1 as a major target, we note that OD01, GD01, and other monoclonal antibodies reported by Sanchez et al. (24) do not cross-react with MACV GP1 or other clade B arenaviruses (22, 24, 35) (Fig. 1*A* and *SI Appendix*, Fig. S9). We suggest that the inability of these antibodies to cross-react with MACV GP1, the most closely related pathogenic NW arenavirus species, may be because of the specific sequence differences and structural variations among the GP1 glycoproteins (Fig. 3). Indeed, this hypothesis is supported by overlay analysis of our eOD01–JUNV GP1 complex with MACV GP1, which indicates major clashes with the elongated helical C-terminal region of the MACV GP1 that would interfere with OD01 recognition (Fig. 2*D* and *SI Appendix*, Fig. S10). Cross-neutralizing antibodies capable of targeting both JUNV and MACV GP1 would likely need to accommodate for the differential presence of these helices, as well as for the sequence variation at the RBS.

Although few JUNV-specific nAbs have been reported to date, Mahmutovic et al. (26) have demonstrated that the hTfR1 binding site on the GP1 glycoprotein is a major target for antibodies generated during natural human infection. Indeed, the overlap of OD01 and GDO01 footprints (Fig. 3) is consistent with the existence of an immunodominant epitope at the RBS of JUNV GP1 (26, 35). As a result, the identification of nAbs targeting other neutralizing epitopes is an important consideration for developing synergetic, noncompeting combinations of therapeutic anti-JUNV mAbs. Indeed, Robinson et al. (36) reported a range of neutralizing epitopes among human mAbs raised upon infection by Lassa virus (LASV), a more distantly related Old World arenavirus. Of the 16 identified anti-LASV nAbs, 13 require the assembled GPC for binding, whereas 3 require only the GP1 (36). Thus, emerging techniques in mAb generation, such as the isolation of antigen-specific B cells (37) against an intact prefusion GPC spike antigen, may reveal antibodies capable of targeting alternative non-RBS epitopes on the JUNV glycoprotein surface.

Materials and Methods

Protein Expression and Purification. The cDNA of JUNV (GenBank accession no. ACO52428), MACV (AAS77647), and LCMV (CAC01231) glycoproteins was synthetized by GeneArt (Life Technologies). For crystallization, a construct of JUNV GP1 (D87–N232) was derived by high-throughput cloning into the pOPINTTGneo mammalian expression vector (38). Constructs of MACV GP1 (E87–F257), LCMV GP1 (M81–K256), and an additional construct of JUNV GP1 with an amino acid C-terminal truncation (D87–V231; to facilitate cloning) were cloned into the pHLsec vector (39) for ELISA experiments. Proteins were expressed in transiently transfected HEK 293T cells (ATCC CRL-1573) in the presence of the α-mannosidase inhibitor, kifunensine, as previously described (39). Cell supernatants were harvested 4 d after transfection, clarified, and diafiltrated against a buffer containing 10 mM Tris (pH 8.0) and 150 mM NaCl (ÄKTA Flux diafiltration system; GE Healthcare). Glycoproteins were purified by immobilized nickel-affinity chromatography (5-mL HisTrap FF crude column and ÄKTA FPLC system; GE Healthcare) followed by size-exclusion chromatography (SEC) using a Superdex 200 10/300 Increase column (GE Healthcare), equilibrated in 10 mM Tris pH 8.0, 150 mM NaCl buffer. To enable crystallogenesis, JUNV GP1 was partially deglycosylated by $endoF_1$ treatment (40). Following deglycosylation, JUNV GP1 was repurified by SEC, as described above.

The mAb, OD01 (clone OD01-AA09), was obtained through BEI Resources (Biodefense and Emerging Infections Research Resources Repository). The Fab fragment of OD01 was produced using the Pierce Mouse IgG1 Fab and F(ab′)2 Preparation Kit (Thermo Fischer Scientific) following the manufacturer's protocol. The eOD01 Fab fragment heavy- and light-chain genes were synthetized by GeneArt (Life Technologies), and the codon optimized cDNAs were cloned into the pHLsec vector (39). A C-terminal His_6-tag was included in the heavy chain construct and both chains were coexpressed [1:1 (wt/wt) ratio of Fab heavy to light chain expressing plasmids] in HEK293T cells and purified, as described above.

For ELISA experiments, the eOD01 Fab fragment variable domains were cloned into human IgG heavy and κ light-chain full-length constant region expression vectors (41). The recombinant antibody was expressed in HEK293 Freestyle cells cotransfected with heavy- and light-chain antibody expressing plasmids at a 1:1 (wt/wt) ratio with PEImax [1:3 (wt/wt) PEI:total DNA; Polysciences]. Transfections were performed according to the manufacturer's protocol, antibody supernatant was harvested 4 d following transfection, and clarified. Chimeric eOD01 antibody was purified over a protein A column, eluted with 0.1 M glycine (pH 3.5), concentrated, and buffer exchanged into PBS.

Crystallization and Structure Determination. Before crystallization, Fab OD01 and JUNV GP1 were mixed in a 1:1.1 molar ratio. Initial OD01 Fab–JUNV GP1 complex crystals were obtained at room temperature using the sitting-drop vapor-diffusion method (42) by mixing 100 nL of protein (at a concentration of 6.0 $mg{\cdot}mL^{-1}$) in 10 mM Tris pH 8.0, 150 mM NaCl buffer with 100 nL of precipitant containing 20% (vol/vol) 2-propanol, 20% (wt/vol) PEG 4000, and 0.1 M trisodium citrate (pH 5.6). Crystallization drops were equilibrated against 95 μL of a precipitant-containing reservoir. X-ray diffraction data were collected from several optimized crystals grown separately in the presence of the precipitant plus one of the following additives: 100 nL 6% (wt/vol) D-trehalose dihydrate (added to the crystallization drop), 100 nL 6% (wt/vol) D-galactose (added to the crystallization drop), or 20 μL 40% (vol/vol) 1-propanol (added to the reservoir).

For crystallization, recombinantly produced Fab eOD01 and JUNV GP1, were mixed at a 1:1.2 molar ratio. After complex formation, excess JUNV GP1 was removed by SEC and the complex was crystallized, as described above. X-ray diffraction data were collected from several optimized crystals grown separately in the presence of the original precipitant plus one of the following additives: 20 μL of 40% (vol/vol) 1-propanol (added to the reservoir) or 40% (vol/vol) acetone (added to the reservoir). Crystals were cryoprotected with 25% (vol/vol) glycerol and flash-frozen in liquid nitrogen.

X-ray data were recorded at Beamline I02 at the Diamond Light Source (Didcot, UK) on a Pilatus 6MF detector (Dectris). X-ray data were indexed, integrated, and scaled with XIA2 (43). The high-resolution cut-off for the data was determined by analysis of $CC_{1/2}$, as defined by Karplus and Diederichs (44). The structure of the OD01–JUNV GP1 complex was phased by molecular replacement with PHASER (45) using the crystal structures of a mouse Fab fragment [PDB ID code 3WII (46)] and MACV GP1 [PDB ID code 2WFO (19)] as search models. Iterative model building was performed with COOT (47) to obtain a model of OD01 Fab with an amino acid sequence that was found to provide the best fit to the experimental electron density (eOD01 sequence). Structure refinement was performed with Refmac5 (48) in the CCP4 suite including translation–libration–screw–rotation restraints (49, 50) and locally defined noncrystallographic symmetry. The eOD01–JUNV GP1 complex structure was determined as described above, except the OD01–JUNV GP1 structure was used for phasing by molecular replacement. The final refined structure was validated with MolProbity (51). Conformational validation of carbohydrate structures was performed using the Privateer software (52).

ELISA Experiments. ELISA plates (High Bind Microplate; Corning) were coated with viral glycoproteins in PBS (3 $\mu g{\cdot}mL^{-1}$) overnight at 4 °C. Plates were washed four times with PBS-T (PBS with 0.05% Tween-20) and blocked for 1 h with 5% nonfat milk in PBS-T. The mouse-derived antibodies [OD01 (clone OD01-AA09), GD01 (clone GD01-AG02), QC03 (clone QC03-BF11), GB03 (clone GB03-BE08), and LD05 (clone LD05-BF09) (24), obtained through BEI Resources] and the purified eOD01 chimeric antibody were serially diluted in 5% nonfat milk/PBS-T and incubated with the viral glycoproteins for 2 h, then plates were washed as above. Mouse-derived antibodies were detected using alkaline phosphatase-conjugated goat anti-mouse IgG (Fab specific) antibody (Sigma), and the chimeric eOD01 antibody was detected using alkaline phosphatase conjugated goat anti-human F(ab′)2 antibody (Thermo Fisher Scientific). Reactions were incubated with the secondary antibody for 1 h and the plates were washed as above. Binding was detected

with the p-nitrophenyl phosphate substrate (Sigma) and the plates were read at 405 nm.

ACKNOWLEDGMENTS. We thank Prof. David Stuart for helpful comments and discussions; the Diamond Light Source for beamtime (proposal MX10627); and the staff of Beamline I02 for support. A.Z. is supported by the European Union Horizon 2020 Marie Curie Fellowship (658363); T.A.B. and K.J.D. are supported by the Medical Research Council (MR/J007897/1, MR/L009528/1, MR/K024426/1, and MR/N002091/1); D.D.P. is supported by the Swiss National Science Foundation (Grant 310030_149340/1); work in the M.C. laboratory is supported by the International AIDS Vaccine Initiative (IAVI), an IAVI Neutralizing Antibody Center Collaboration for AIDS Vaccine Discovery grant, and the Scripps Center for HIV/AIDS Vaccine Immunology and Immunogen Discovery (1UM1AI100663); J.H.N. is supported by NIH Grant R15 AI119803; and The Wellcome Trust Centre for Human Genetics is supported by Wellcome Trust Centre Grant 203141/Z/16/Z. The following reagents were obtained through the NIH Biodefense and Emerging Infections Research Resources Repository, National Institute of Allergy and Infectious Diseases, NIH: monoclonal anti-Junin virus, clone OD01-AA09 (IgG, mouse), NR-2567; monoclonal anti-Junin virus, clone GD01-AG02 (produced in vitro), NR-43776; monoclonal anti-Junin virus, clone QC03-BF11 (produced in vitro), NR-43775; monoclonal anti-Junin virus, clone GB03-BE08 (produced in vitro), NR-43227; and monoclonal anti-Junin virus, clone LD05-BF09 (produced in vitro), NR-48833.

1. Shao J, Liang Y, Ly H (2015) Human hemorrhagic fever causing arenaviruses: Molecular mechanisms contributing to virus virulence and disease pathogenesis. *Pathogens* 4:283–306.
2. Radoshitzky SR, et al. (2015) Past, present, and future of arenavirus taxonomy. *Arch Virol* 160:1851–1874.
3. McLay L, Liang Y, Ly H (2014) Comparative analysis of disease pathogenesis and molecular mechanisms of New World and Old World arenavirus infections. *J Gen Virol* 95:1–15.
4. Delgado S, et al. (2008) Chapare virus, a newly discovered arenavirus isolated from a fatal hemorrhagic fever case in Bolivia. *PLoS Pathog* 4:e1000047.
5. Lisieux T, et al. (1994) New arenavirus isolated in Brazil. *Lancet* 343:391–392.
6. Enserink M (2000) Emerging diseases. New arenavirus blamed for recent deaths in California. *Science* 289:842–843.
7. García JB, et al. (2000) Genetic diversity of the Junin virus in Argentina: Geographic and temporal patterns. *Virology* 272:127–136.
8. Gómez RM, et al. (2011) Junín virus. A XXI century update. *Microbes Infect* 13: 303–311.
9. Geisbert TW, Jahrling PB (2004) Exotic emerging viral diseases: Progress and challenges. *Nat Med* 10(12, Suppl):S110–S121.
10. Maiztegui JI, Fernandez NJ, de Damilano AJ (1979) Efficacy of immune plasma in treatment of Argentine haemorrhagic fever and association between treatment and a late neurological syndrome. *Lancet* 2:1216–1217.
11. Maiztegui JI, et al.; AHF Study Group (1998) Protective efficacy of a live attenuated vaccine against Argentine hemorrhagic fever. *J Infect Dis* 177:277–283.
12. Enria DA, Briggiler AM, Fernandez NJ, Levis SC, Maiztegui JI (1984) Importance of dose of neutralising antibodies in treatment of Argentine haemorrhagic fever with immune plasma. *Lancet* 2:255–256.
13. York J, Nunberg JH (2016) Myristoylation of the arenavirus envelope glycoprotein stable signal peptide is critical for membrane fusion but dispensable for virion morphogenesis. *J Virol* 90:8341–8350.
14. Nunberg JH, York J (2012) The curious case of arenavirus entry, and its inhibition. *Viruses* 4:83–101.
15. Burri DJ, da Palma JR, Kunz S, Pasquato A (2012) Envelope glycoprotein of arenaviruses. *Viruses* 4:2162–2181.
16. Li S, et al. (2016) Acidic pH-Induced conformations and LAMP1 binding of the Lassa virus glycoprotein spike. *PLoS Pathog* 12:e1005418.
17. Parsy ML, Harlos K, Huiskonen JT, Bowden TA (2013) Crystal structure of Venezuelan hemorrhagic fever virus fusion glycoprotein reveals a class 1 postfusion architecture with extensive glycosylation. *J Virol* 87:13070–13075.
18. Crispin M, Zeltina A, Zitzmann N, Bowden TA (2016) Native functionality and therapeutic targeting of arenaviral glycoproteins. *Curr Opin Virol* 18:70–75.
19. Bowden TA, et al. (2009) Unusual molecular architecture of the machupo virus attachment glycoprotein. *J Virol* 83:8259–8265.
20. Radoshitzky SR, et al. (2007) Transferrin receptor 1 is a cellular receptor for New World haemorrhagic fever arenaviruses. *Nature* 446:92–96.
21. Bowden TA, Jones EY, Stuart DI (2011) Cells under siege: Viral glycoprotein interactions at the cell surface. *J Struct Biol* 175:120–126.
22. Abraham J, Corbett KD, Farzan M, Choe H, Harrison SC (2010) Structural basis for receptor recognition by New World hemorrhagic fever arenaviruses. *Nat Struct Mol Biol* 17:438–444.
23. Choe H, Jemielity S, Abraham J, Radoshitzky SR, Farzan M (2011) Transferrin receptor 1 in the zoonosis and pathogenesis of New World hemorrhagic fever arenaviruses. *Curr Opin Microbiol* 14:476–482.
24. Sanchez A, et al. (1989) Junin virus monoclonal antibodies: Characterization and cross-reactivity with other arenaviruses. *J Gen Virol* 70:1125–1132.
25. Zeitlin L, et al. (2016) Monoclonal antibody therapy for Junin virus infection. *Proc Natl Acad Sci USA* 113:4458–4463.
26. Mahmutovic S, et al. (2015) Molecular basis for antibody-mediated neutralization of New World hemorrhagic fever mammarenaviruses. *Cell Host Microbe* 18:705–713.
27. Martin AC, Thornton JM (1996) Structural families in loops of homologous proteins: Automatic classification, modelling and application to antibodies. *J Mol Biol* 263: 800–815.
28. Sommerstein R, et al. (2015) Arenavirus glycan shield promotes neutralizing antibody evasion and protracted infection. *PLoS Pathog* 11:e1005276.
29. Swindells MB, et al. (2017) abYsis: Integrated antibody sequence and structure-management, analysis, and prediction. *J Mol Biol* 429:356–364.
30. Abraham J, et al. (2009) Host-species transferrin receptor 1 orthologs are cellular receptors for nonpathogenic new world clade B arenaviruses. *PLoS Pathog* 5: e1000358.
31. Radoshitzky SR, et al. (2008) Receptor determinants of zoonotic transmission of New World hemorrhagic fever arenaviruses. *Proc Natl Acad Sci USA* 105:2664–2669.
32. Scheid JF, et al. (2011) Sequence and structural convergence of broad and potent HIV antibodies that mimic CD4 binding. *Science* 333:1633–1637.
33. Schmidt AG, et al. (2015) Viral receptor-binding site antibodies with diverse germline origins. *Cell* 161:1026–1034.
34. Chen Z, et al. (2013) Cross-neutralizing human anti-poliovirus antibodies bind the recognition site for cellular receptor. *Proc Natl Acad Sci USA* 110:20242–20247.
35. Brouillette RB, Phillips EK, Ayithan N, Maury W (2017) Differences in glycoprotein complex (GPC) receptor binding site accessibility prompt poor cross-reactivity of neutralizing antibodies between closely related arenaviruses. *J Virol* 91:e01454-16.
36. Robinson JE, et al. (2016) Most neutralizing human monoclonal antibodies target novel epitopes requiring both Lassa virus glycoprotein subunits. *Nat Commun* 7: 11544.
37. Smith K, et al. (2009) Rapid generation of fully human monoclonal antibodies specific to a vaccinating antigen. *Nat Protoc* 4:372–384.
38. Berrow NS, Alderton D, Owens RJ (2009) The precise engineering of expression vectors using high-throughput In-Fusion PCR cloning. *Methods Mol Biol* 498:75–90.
39. Aricescu AR, Lu W, Jones EY (2006) A time- and cost-efficient system for high-level protein production in mammalian cells. *Acta Crystallogr D Biol Crystallogr* 62: 1243–1250.
40. Chang VT, et al. (2007) Glycoprotein structural genomics: Solving the glycosylation problem. *Structure* 3:267–273.
41. Tiller T, et al. (2008) Efficient generation of monoclonal antibodies from single human B cells by single cell RT-PCR and expression vector cloning. *J Immunol Methods* 329: 112–124.
42. Walter TS, et al. (2005) A procedure for setting up high-throughput nanolitre crystallization experiments. Crystallization workflow for initial screening, automated storage, imaging and optimization. *Acta Crystallogr D Biol Crystallogr* 61:651–657.
43. Winter G (2009) xia2: An expert system for macromolecular crystallography data reduction. *J Appl Crystallogr* 43:186–190.
44. Karplus PA, Diederichs K (2012) Linking crystallographic model and data quality. *Science* 336:1030–1033.
45. McCoy AJ, et al. (2007) Phaser crystallographic software. *J Appl Crystallogr* 40: 658–674.
46. Nakayama T, et al. (2015) Structural features of interfacial tyrosine residue in ROBO1 fibronectin domain-antibody complex: Crystallographic, thermodynamic, and molecular dynamic analyses. *Protein Sci* 24:328–340.
47. Emsley P, Cowtan K (2004) Coot: Model-building tools for molecular graphics. *Acta Crystallogr D Biol Crystallogr* 60:2126–2132.
48. Murshudov GN, et al. (2011) REFMAC5 for the refinement of macromolecular crystal structures. *Acta Crystallogr D Biol Crystallogr* 67:355–367.
49. Winn MD, Murshudov GN, Papiz MZ (2003) Macromolecular TLS refinement in REFMAC at moderate resolutions. *Methods Enzymol* 374:300–321.
50. Painter J, Merritt EA (2006) Optimal description of a protein structure in terms of multiple groups undergoing TLS motion. *Acta Crystallogr D Biol Crystallogr* 62: 439–450.
51. Chen VB, et al. (2010) MolProbity: All-atom structure validation for macromolecular crystallography. *Acta Crystallogr D Biol Crystallogr* 66:12–21.
52. Agirre J, et al. (2015) Privateer: Software for the conformational validation of carbohydrate structures. *Nat Struct Mol Biol* 22:833–834.
53. Ren J, et al. (2009) DOG 1.0: Illustrator of protein domain structures. *Cell Res* 19: 271–273.
54. Krissinel E, Henrick K (2007) Inference of macromolecular assemblies from crystalline state. *J Mol Biol* 372:774–797.
55. Sievers F, et al. (2011) Fast, scalable generation of high-quality protein multiple sequence alignments using Clustal Omega. *Mol Syst Biol* 7:539.
56. Robert X, Gouet P (2014) Deciphering key features in protein structures with the new ENDscript server. *Nucleic Acids Res* 42:W320–W324.